Sarah Kim
School of Chemical and Biomolecular Engineering, Georgia Institute of Technology, Atlanta, GA 30332

Yoon Jo Kim
Department of Mechanical Engineering, Washington State University, Vancouver, WA 98686

Yogendra K. Joshi

Andrei G. Fedorov

The George Woodruff School of Mechanical Engineering, Georgia Institute of Technology, Atlanta, GA 30332

Paul A. Kohl[1]
School of Chemical and Biomolecular Engineering, Georgia Institute of Technology, Atlanta, GA 30332
e-mail: kohl@gatech.edu

Absorption Heat Pump/Refrigeration System Utilizing Ionic Liquid and Hydrofluorocarbon Refrigerants

The ionic liquid butylmethylimidazolium hexafluorophosphate (bmim)(PF_6) and five different hydrofluorocarbon refrigerants were investigated as the working fluid pairs for a waste-heat driven absorption heat pump system for possible applications in electronics thermal management. A significant amount of the energy consumed in large electronic systems is used for cooling, resulting in low grade waste heat, which can be used to drive an absorption refrigeration system if a suitable working fluids can be identified. The Redlich–Kwong-type equation of state was used to model the thermodynamic conditions and the binary mixture properties at the corresponding states. The effects of desorber and absorber temperatures, waste-heat quality, and system design on the heat pump performance were investigated. Supporting experiments using R134a/(bmim)(PF_6) as the working fluid pair were performed. Desorber and absorber outlet temperatures were varied by adjusting the desorber supply power and the coolant temperature at the evaporator inlet, respectively. For an evaporator temperature of 41 °C, which is relevant to electronics cooling applications, the maximum cooling-to-total-energy input was 0.35 with the evaporator cooling capability of 36 W and the desorber outlet temperature in the range of 50 to 110 °C. [DOI: 10.1115/1.4007111]

1 Introduction

The energy consumption of large scale information technology equipment and infrastructure, such as data centers, has been increasing, as the demand for computing and storage capacity rises. The Environmental Protection Agency reported that the energy consumption of servers and data centers in 2006 was more than double that consumed in year 2000 [1]. Cooling is one of the major factors in total energy consumption in data centers accounting for about 30%–50% of the total power drawn from the grid [2]. A variety of novel alternative thermal solutions for electronics cooling have been reported, including thermosyphon [3], loop heat pipes [4], electroosmotic pumping [5], stacked microchannels [6], impinging jets [7], thermoelectric microcoolers [8], vapor compression refrigeration [9], and absorption based refrigeration systems [10,11]. The cooling systems can be categorized into passive and active; passive cooling systems utilize capillary or gravitational force to circulate the working fluid. Active cooling systems are driven by a pump or a compressor for augmented cooling capacity and improved performance. Active systems driven by a compressor, refrigeration/heat pump systems, offer a further increase in heat removal by insertion of a negative thermal resistance into heat flow path [9]. Among the different candidate technologies, absorption refrigeration offers the compactness, relative ease of scalability to varying cooling load, and relatively high coefficient of performance (COP) (assuming waste heat is available), making it an attractive option for cooling of high power, high performance electronics [12]. In places where an excess of heat of sufficient quality is available, absorption refrigeration offers an opportunity to recycle the thermal energy, which would otherwise be wasted.

Commonly used absorption refrigeration working fluid pairs, ammonia/water and water/LiBr, have drawbacks including toxicity (ammonia), negative effects of crystallization (LiBr), incompatibility with metal components, and necessity for a rectifier for postdesorption separation of fluid streams [13]. Ethylene g,lycol/water were selected as working fluids in an experimental absorption cycle [14], however, water as a refrigerant has several disadvantages including high vapor pressure, subatmospheric pressure conditions and restricted temperature range in system operation. Ionic liquids (ILs) are a liquid salt at ambient temperature. ILs have been considered as promising absorbents because of their tunable properties, zero vapor pressure, high thermal stability, and environmental safety [15]. In particular, the low volatility of ionic liquid enables easy separation of the working fluids by thermal stratification. However, no experimental investigations on the refrigeration/heat pump system performance with an IL as a working fluid have yet been undertaken, despite several theoretical reports in the literature [15–17]. This is perhaps due to the limited information on the thermodynamic and transport properties of ILs and IL/refrigerant mixtures for the temperatures and pressures that are relevant to operation of the heat pump/refrigeration systems, which makes the system and component design challenging.

As the first step in addressing this challenge, in this work the butylmethylimidazolium hexafluorophosphate (bmim)(PF_6) IL with several hydrofluorocarbon (HFC) refrigerants were studied as working pairs for an absorption refrigeration cycle. The Redlich–Kwong (RK) equation of state (EOS) was employed for thermodynamic property correlation in order to predict the solubility and enthalpy of the binary IL/refrigerant mixtures. Using the RK formalism, a 40 W capacity refrigeration/heat pump system was theoretically evaluated for the best performance using several metrics. In support of the theoretical investigation, a laboratory scale experimental prototype was also designed, built, and operated using (bmim)(PF_6) and R134a, one of the most commonly used refrigerants with zero ozone-depletion-potential. The principal goal of the experimental investigation was to establish

[1]Corresponding author.

Contributed by Electronic and Photonic Packaging Division of ASME for publication in the Journal of Electronic Packaging. Manuscript received March 12, 2012; final manuscript received June 26, 2012; published online July 20, 2012. Assoc. Editor: Amy Fleischer.

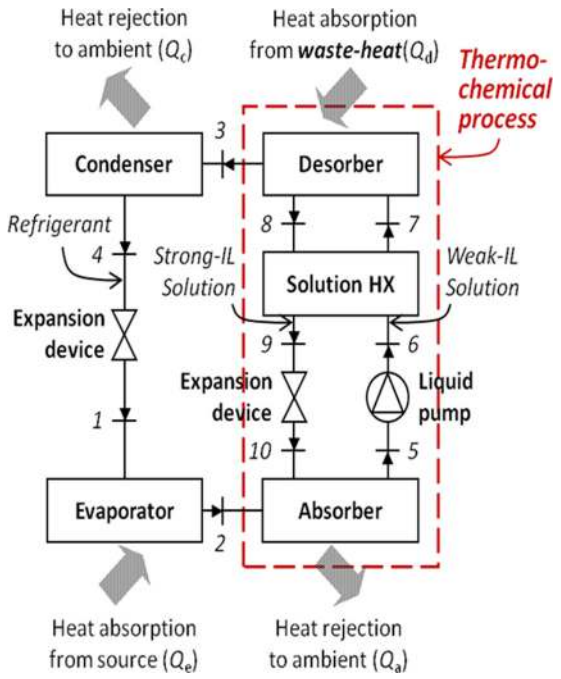

Fig. 1 Schematic diagram of an absorption refrigeration system using IL/refrigerant mixture as a working fluid

feasibility of the absorption heat pump system using IL/refrigerant working fluid pair and to evaluate the system performance as a function of control inputs, such as power input to the desorber, and the evaporator temperature. The friction loss and pumping power consumption of the absorption system using various working fluids were evaluated separately [18].

2 Thermodynamic Model

The principal features of the absorption refrigeration cycle are shown in Fig. 1. The cycle resembles that of the vapor compression refrigeration (heat pump) system, except the vapor compressor is replaced with a thermochemical process consisting of an absorber, a liquid pump, a solution heat exchanger, a desorber, and an expansion device. The pressurization in the thermochemical process starts in the absorber, where the refrigerant vapor from the evaporator (state point 2) is exothermically absorbed into the strong-IL solution (state point 10), resulting in a weak IL solution at state point 5. The IL solution is pressurized by the liquid pump after the absorber. Then, the solution (regenerative) heat exchanger preheats the weak-IL solution at state point 6 creating state point 7 using heat from the strong-IL solution flowing back to the absorber (from the desorber). In the desorber, high pressure and high temperature superheated refrigerant vapor is released from the IL via desorption from the weak-IL solution by the addition of heat (preferably high quality waste heat). The strong-IL returns to the absorber through the solution heat exchanger and an expansion device. The condensation/absorption process at the absorber and vaporization/desorption process at the desorber both occur in the liquid phase. This allows use of a liquid pump to create the pressure difference between condenser and evaporator. Although the presence of the absorber and desorber increases the overall system volume, the displacement volume and power consumption for liquid compression are much smaller than those for vapor compression. Table 1 summarizes the main components/processes of an absorption heat pump system using IL/refrigerant mixture as a working fluid.

Benchmarking of the refrigerant/ionic liquid combination and system-level simulations were carried out. Energy and mass conservation equations for all components comprising the system

Table 1 Main components and the processes of an absorption refrigeration system using IL/refrigerant as working fluids

Component	State	Process
Evaporator	$1 \rightarrow 2$	Heat absorption from chip
Absorber	$2, 10 \rightarrow 5$	Refrigerant absorption/condensation into IL
Pump	$5 \rightarrow 6$	Isentropic pressurization
Solution HX	$6 \rightarrow 7, 8 \rightarrow 9$	Regenerative preheating
Desorber	$7 \rightarrow 8, 3$	Refrigerant desorption/vaporization from IL
Condenser	$3 \rightarrow 4$	Heat rejection to ambient
Expansion device	$4 \rightarrow 1, 9 \rightarrow 10$	Isenthalpic expansion

were simultaneously solved to determine the heat and workloads. The overall energy balance for the system is given in Eq. (1):

$$Q_d + Q_e + W_p = Q_c + Q_a \tag{1}$$

where W_p is the liquid pump work and Q is the heat input/output. The subscripts d, e, c, and a represent the desorber, evaporator, condenser, and absorber, respectively. All values of heat are expressed as positive (magnitude) values regardless of the direction (in or out) of heat flow. The solution heat exchanger is assumed to be ideal, i.e., to follow an isobaric process and with 100% heat exchanger efficiency. The energy conservation for a subsystem consisting of a regenerative heat exchanger and a pump is given by Eq. (2):

$$(h_9 - h_8)(m_w - m_r) = (h_7 - h_5)m_w - W_p \tag{2}$$

where h is enthalpy; the subscript numbers correspond to the locations shown in the system diagram, Fig. 1, and m_w and m_r are mass flow rates of the weak-IL solution and refrigerant leaving the desorber. Energy conservation for the desorber is given by Eq. (3)

$$Q_d = h_8(m_w - m_r) + h_3 m_r - h_7 m_w \tag{3}$$

Similarly, heat rejected at the absorber is given by Eq. (4):

$$Q_a = h_5 m_w - h_{10}(m_w - m_r) - h_2 m_r \tag{4}$$

Energy conservation for the condenser and the evaporator yield the respective heat loads, Eqs. (5) and (6):

$$Q_c = (h_4 - h_3)m_r \tag{5}$$

$$Q_e = (h_2 - h_1)m_r \tag{6}$$

The cooling-to-total-energy (CE) is then defined as the heat removed at the evaporator divided by the power supplied to the desorber and the pump, Eq. (7):

$$\mathrm{CE} = Q_e/(Q_d + W_p) \tag{7}$$

In this analysis, the RK equation of state (EOS) was used to calculate the thermodynamic properties of the fluids. Binary interaction parameters were introduced to improve the accuracy of the model. Several assumptions were made for convenience in computation: (1) pressure drops in the system heat exchangers are neglected; (2) the expansion process is isenthalpic; (3) the compression process is isentropic; (4) state 4 is saturated liquid refrigerant; (5) state 2 is saturated vapor refrigerant; and (6) the vapor quality at state 10 and state 5 is zero.

The general RK–EOS can be written in the following form, Eqs. (8)–(10) [19]:

Table 2 EOS constants of (bmim)(PF_6) and HFC refrigerants

Pure compound	T_c (K)	P_c (kPa)	β_0	β_1	β_2	β_3
(bmim)(PF_6) [22]	860.5	2645	1.0	0.62627	0	0
R32 [16]	351.26	5782	1.0019	0.48333	−0.07538	0.00673
R125 [16]	339.19	3637	1.0001	0.47736	−0.01977	−0.0177
R134a [16]	374.21	4059	1.0025	0.50532	−0.04983	0
R143a [16]	346.20	3759	1.0006	0.45874	−0.04846	−0.0143
R152a [16]	386.44	4520	1.0012	0.48495	−0.08508	0.0146

$$P = \frac{RT}{V-b} - \frac{a(T)}{V(V+b)} \tag{8}$$

$$a(T) = 0.42748\frac{R^2T_c^2}{P_c}\alpha(T) \tag{9}$$

$$b = 0.08664\frac{RT_c}{P_c} \tag{10}$$

The subscript c represents the critical properties of the substance. P is the pressure, T is the temperature, V is the molar volume, R is the gas constant, and a and b are constants. The temperature-dependent function of the α parameter is expressed by Eq. (11):

$$\alpha(T) = \sum_{k=0}^{\leq 3} \beta_k (1/T_r - T_r)^k, \quad T_r \equiv T/T_c \tag{11}$$

The parameter β_k is determined so as to yield the vapor pressure of each pure compound, the refrigerant and the ionic liquid alone [16]. The critical properties along with β values are summarized in Table 2.

Three binary interaction parameters (BIPs) τ, l, and k were introduced in the a and b parameters for N component mixtures [20].

$$a = \sum_{i,j=1}^{N} \sqrt{a_i a_j} f_{ij}(T)(1-l_{ij})x_i x_j, \quad a_i = 0.42748\frac{R^2T_{ci}^2}{P_{ci}}\alpha(T) \tag{12}$$

$$f_{ij}(T) = 1 + \tau_{ij}/T, \quad \text{where} \quad \tau_{ij} = \tau_{ji} \quad \text{and} \quad \tau_{ii} = 0 \tag{13}$$

$$b = \frac{1}{2}\sum_{i,j=1}^{N} (b_i + b_j)(1-l_{ij})(1-k_{ij})x_i x_j, \quad b_i = 0.08664\frac{RT_{ci}}{P_{ci}} \tag{14}$$

where, $l_{ij} = l_{ji}$; $l_{ii} = 0$; $k_{ij} = k_{ji}$; $k_{ii} = 0$.

At equilibrium for an N-component system, the chemical potential of each species/phase must be the same giving Eq. (15):

$$x_i^\alpha \phi_i^\alpha = x_i^\beta \phi_i^\beta = x_i^\gamma \phi_i^\gamma = \ldots, \quad (i = 1, \ldots, N) \tag{15}$$

where $x_i^\alpha, x_i^\beta, x_i^\gamma, \ldots$ are the mole fractions of the i-th species in the $\alpha, \beta, \gamma, \ldots$ coexisting phases and $\phi_i^\alpha, \phi_i^\beta, \phi_i^\gamma, \ldots$ are the fugacity coefficients of the i-th species in the $\alpha, \beta, \gamma, \ldots$ corresponding phases. The fugacity coefficient can be calculated from Ref. [20]:

$$\ln \varphi_i = \int_V^\infty \left\{ \left(\frac{\partial(nZ)}{\partial n_i} \right)_{T,nV,n_j} - 1 \right\} \frac{dV}{V} - \ln Z \tag{16}$$

$$Z = \frac{PV}{RT} \tag{17}$$

The equilibrium condition, Eq. (15), is used to compute the solubility of a refrigerant in an IL at a given temperature and pressure. An iterative computational code was used to find the BIPs for each binary working fluid mixture of a refrigerant and an IL.

Table 3 Binary interaction parameters for (bmim)(PF_6) and HFC refrigerants

Fluid pair	$l_{12} = l_{21}$	k_{12}	τ_{12} (K)	ΔP(MPa)[a]
R32/(bmim)(PF_6)	0.0295	−0.0167	13.9407	0.010
R125/(bmim)(PF_6)	0.1865	−0.2545	78.5937	0.009
R134a/(bmim)(PF_6)	0.1278	−0.1504	41.9269	0.005
R143a/(bmim)(PF_6)	−0.239	0.1948	50.1348	0.004
R152a/(bmim)(PF_6)	−0.2496	0.2112	70.1631	0.006

[a]Standard deviations of nonlinear least squares in pressures

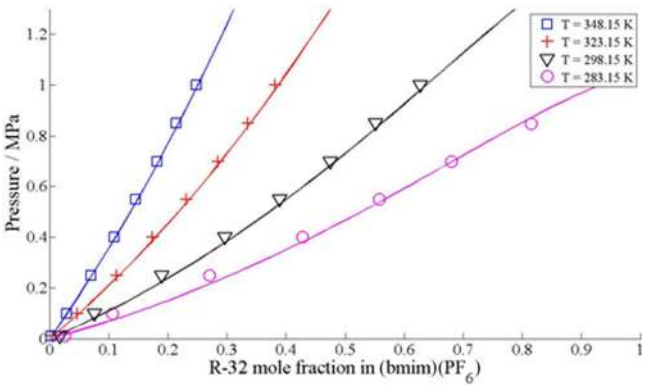

Fig. 2 R32 solubility in (bmim)(PF_6) as a function of temperature (K) and pressure (MPa). Symbols: experimental solubility data [21]; lines: computed EOS model using BIPs.

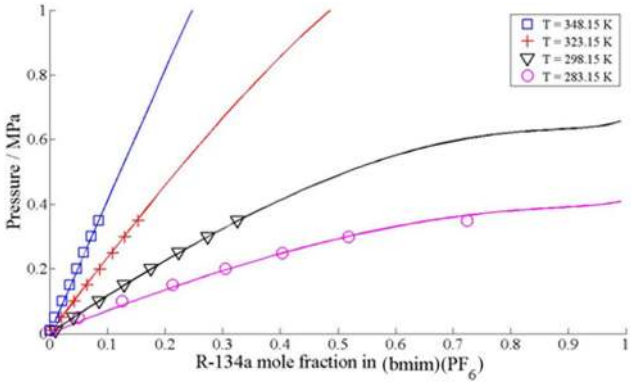

Fig. 3 R134a solubility in (bmim)(PF_6) as a function of temperature (K) and pressure (MPa). Symbols: experimental solubility data [21]; lines: computed EOS model using BIPs.

The objective function was to minimize the nonlinear least square difference between the computed pressure and measured pressure value with the equilibrium condition (Eq. (15)) used as a constraint. The solubility data for HFC and (bmim)(PF_6) mixtures are taken from Shiflett and Yokozeki [21]. The optimum BIPs found for different working fluids are summarized in Table 3.

The BIPs found were used to generate a solubility plot at different temperature and pressure conditions. Figures 2–6 show the solubility of various HFCs in (bmim)(PF_6), where the different lines are isotherms modeled by the EOS, and the symbols indicate experimental data at the same temperatures used to develop the EOS correlations. It can be seen that the quality of the RK correlation is adequate for an entire range of experimental parameters to be useful for the system performance calculations.

The EOS was then used to find the enthalpy values at the point of interest, Eq. (18):

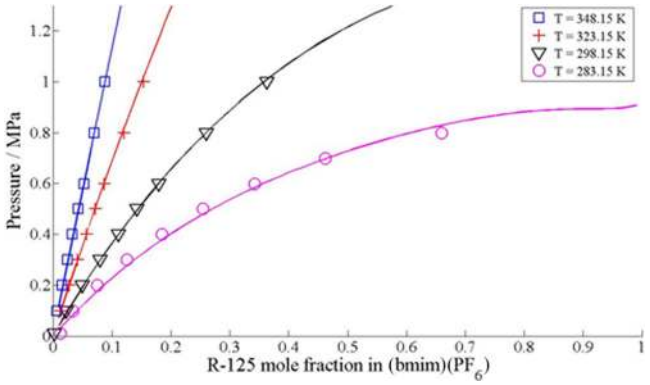

Fig. 4 R125 solubility in (bmim)(PF_6) as a function of temperature (K) and pressure (MPa). Symbols: experimental solubility data [21]; lines: computed EOS model using BIPs.

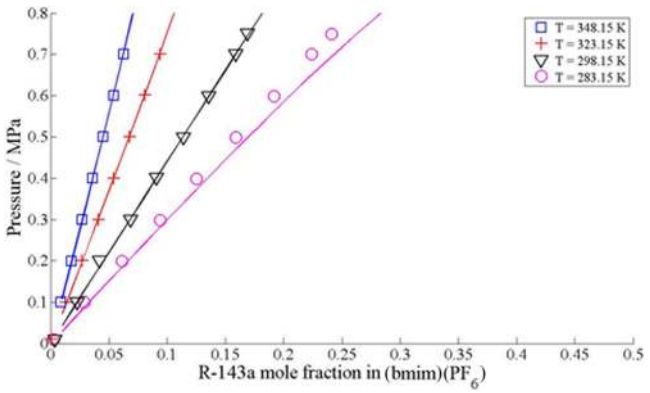

Fig. 5 R143a solubility in (bmim)(PF_6) as a function of temperature (K) and pressure (MPa). Symbols: experimental solubility data [21]; lines: computed EOS model using BIPs.

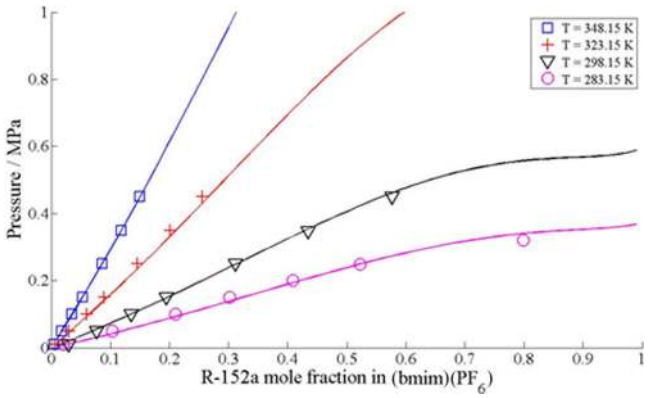

Fig. 6 R152a solubility in (bmim)(PF_6) as a function of temperature (K) and pressure (MPa). Symbols: experimental solubility data [21]; lines: computed EOS model using BIPs.

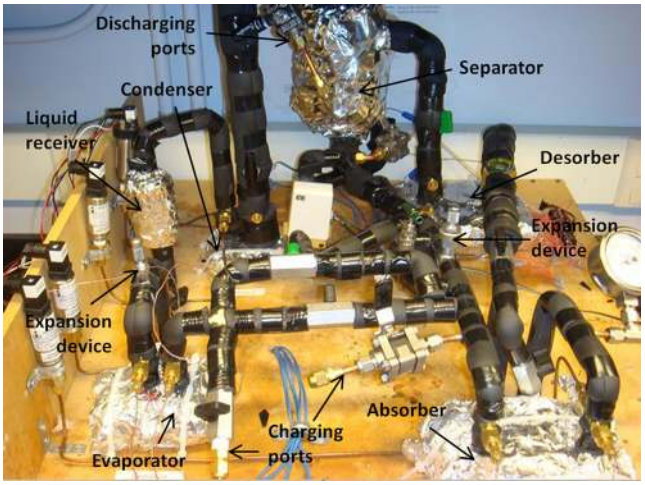

Fig. 7 Experimental test setup for absorption refrigeration system using R134a/(bmim)(PF_6) mixture as a working fluid

$$H = H^R + \int_{T_0}^{T} \sum_{i=1}^{N} x_i C_{pi}^0 dT + H_0 \tag{18}$$

where H^R is the residual enthalpy, T_0 is the reference temperature set as 273.15 K, and H_0 is an arbitrary constant (an enthalpy at the reference state). The ideal-gas heat capacity of the i-th species, C_{pi}^o, is modeled in Eq. (19):

$$C_{pi}^0 = C_{pi}^0 + C_{pi}^1 T + C_{pi}^2 T^2 + C_{pi}^3 T^3 \tag{19}$$

The coefficients in Eq. (19) are given in Table 4. Using the heat capacity for each species in the mixture, the enthalpy for the RK–EOS is given by Eq. (20):

$$H = \left(\frac{a}{b} - \frac{T}{b}\frac{da}{dT}\right) \ln \frac{V}{V+b} + RT(Z-1) + \int_{T_0}^{T} \sum_{i=1}^{N} x_i C_{pi}^0 dT + H_0 \tag{20}$$

3 Experimental

An experimental setup for a laboratory scale absorption refrigeration system using R134a/(bmim)(PF_6) mixture as a working fluid was built and operated, as shown in Fig. 7. The microfluidic channel heat/mass exchangers were fabricated in copper and used for an evaporator, a condenser, an absorber, and a desorber. A magnetic gear pump was employed for the circulation of the R134a/(bmim)(PF_6) mixture. A 150 ml stainless-steel cylinder was installed for the separation of refrigerant-vapor from the mixture. Vapor/noncondensables were trapped in the 50 ml liquid-receiver located at the outlet of the condenser to guarantee liquid flow through the expansion device. Orifice-type metering valves were adopted for the expansion devices for fine adjustment of

Table 4 Coefficients for ideal gas heat capacity of pure compounds ($J \cdot mol^{-1}$)

Pure compound	C_p^0 ($J \cdot mol^{-1}$)	C_p^1 ($J \cdot mol^{-1}K^{-1}$)	C_p^2 ($J \cdot mol^{-1}K^{-2}$)	C_p^3 ($J \cdot mol^{-1}K^{-3}$)
(bmim)(PF_6) [15]	−2.214	0.57685	-3.854×10^{-4}	9.785×10^{-8}
R32 [16]	20.34	0.07534	1.872×10^{-5}	-3.116×10^{-8}
R125 [16]	16.58	0.33983	-2.873×10^{-4}	8.870×10^{-8}
R134a [16]	12.89	0.30500	-2.342×10^{-4}	6.852×10^{-8}
R143a [16]	5.740	0.31388	-2.595×10^{-4}	8.410×10^{-8}
R152a [16]	8.670	0.2394	-1.456×10^{-4}	3.392×10^{-8}

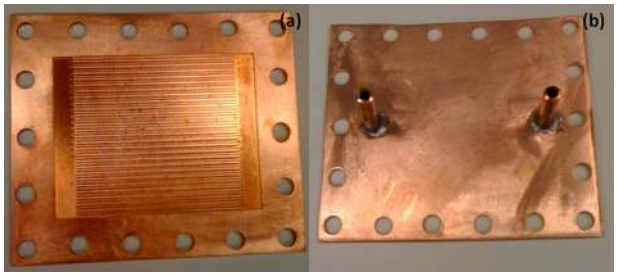

Fig. 8 (*a*) Absorber microchannel and (*b*) cover plate with inlet and outlet ports

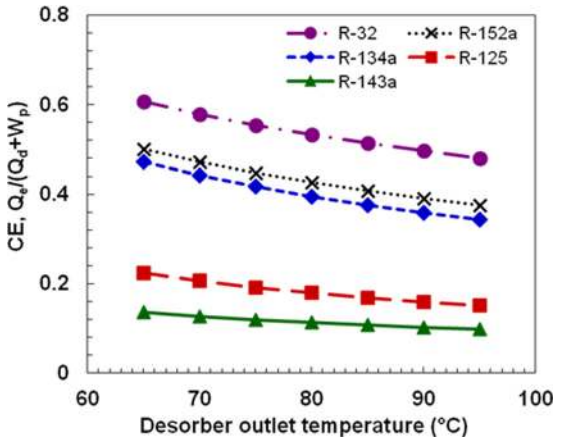

Fig. 9 Desorber outlet temperature effect on system performance for working fluid (bmim)(PF_6) and HFC refrigerants. $T_c/T_e/T_a = 50/25/35\,^{\circ}C$

flow rates, as well as the system cooling capability. Kapton heaters were attached on the backsides of the evaporator and desorber to simulate the heat dissipation from chip, and waste heat as an energy source, respectively. The absorber and the condenser were cooled by secondary water loops. Pressure transducers were placed at the evaporator inlet, the absorber outlet, the desorber intlet, the condenser outlet, and the separator mixture outlet. The temperatures at the inlets and outlets of all components were measured using T-type (copper-constantan) thermocouples. The heat/mass exchangers, the separator and the liquid-receiver were insulated using glass-fiber insulation. The copper tubes (0.635 cm) were thermally insulated using elastomeric material (ethylene propylene terpolymer). As shown in Fig. 8, the heat/mass exchangers have microchannels with 1 mm × 1 mm cross-sectional area and the channel pitch of 1.5 mm. The evaporator and condenser have channel lengths of 1.5 cm and 3 cm, respectively, while the absorber and desorber have the channel lengths of 5 cm. Relatively large cross-sectional area of the absorber and the desorber was allowed to reduce the pressure drop due to the high viscosity of ILs.

To investigate the effect of desorber power (waste heat) input on the evaporator cooling capacity (varied up to ~40 W), the desorber power has been increased up to ~200 W to keep the evaporator temperature constant at 41 °C with the condenser and absorber coolant (secondary fluid) inlet temperatures of 22 °C. In addition, the effects of absorber and condenser coolant inlet temperatures were also investigated by varying both coolant inlet temperatures between 30 °C and 45 °C with the desorber power maintained at 120 W. The measured parameters were temperature, absolute pressure, and electrical power input. Uncertainty in the temperature reading was 0.1 K for calibrated thermocouples relative to each other. The uncertainty in absolute pressure measurement was 0.25% of the maximum range 2068.43 kPa (300 psi). The uncertainty in the output value of the electrical power transducer is given as 0.14% of the measured value. The heat transfer at the evaporator Q_e and desorber Q_d were measured in the experimental setup. The ratio of Q_e/Q_d is defined here as CE_{Th}, which is the same as CE in Eq. (7) except the liquid pump work has been neglected, giving Eq. (21):

$$CE_{Th} = \frac{Q_e}{Q_d} \tag{21}$$

The pumping work was ignored in Eq. (21) because the experimental system was not designed for efficient pumping due to the excessive use of sensors and piping. In addition, the pumping work is normally a very minor part of the total energy input (denominator of Eq. (7)). Applying error propagation analysis to Eq. (21) gives the estimated uncertainty of 0.2%.

4 Results and Discussion

The system efficiency was evaluated at different desorber outlet temperatures (T_8), which is the highest operating temperature in the system. The temperature of the heat source (e.g., waste heat) for powering the system needs to be higher than this temperature. Lower desorber outlet temperature is, therefore, preferred to utilize low thermodynamic quality waste heat. Figure 9 shows the effect of desorber outlet temperature on CE where the condenser and evaporator saturation temperatures are set as 50 °C and 25 °C, respectively, while the absorber outlet temperature was maintained at 35 °C. The state conditions, along with the CE value at a desorber outlet temperature of 80 °C are summarized in Table 5. The circulation ratio is defined as $f = m_w/m_r$ and x_s and x_w are the refrigerant mole fractions in the strong and weak mixture solutions, respectively. The two operating pressure conditions are determined by the saturated pressures at the corresponding condenser and evaporator temperatures. At high desorber temperatures, the CE tends to decrease, as more cooling will be required to maintain the desired condenser and absorber operating temperatures. Also, the remaining refrigerant content in the strong-IL solution is sufficiently low at high temperatures and the impact of a further increased desorber outlet temperature on the cooling capacity is small. Eq. (3) can be rewritten as Eq. (22):

$$\frac{Q_d}{m_r} = f(h_8 - h_7) - h_8 + h_3 \tag{22}$$

The desorber outlet temperature changes both the enthalpies and the circulation ratio in Eq.(22). An increase in the desorber outlet temperature increases the enthalpies (h_3 and h_8), which

Table 5 Theoretical performances and state conditions ($T_a/T_c/T_e/T_d = 35/50/25/80\,^{\circ}C$, $Q_e = 100$ W)

Fluid pair	P_c, P_d (kPa)	P_e, P_a (kPa)	f	x_s (mole %)	x_w (mole %)	Q_d (W)	CE
R32/(bmim)(PF_6)	3144	1688	4.40	55.9	76.4	184.9	0.533
R125/(bmim)(PF_6)	2540	1376	9.48	20.6	36.2	542.4	0.180
R134a/(bmim)(PF_6)	1319	665	6.60	29.4	49.7	250.7	0.395
R143a/(bmim)(PF_6)	2310	1262	47.0	17.3	22.3	842.5	0.114
R152a/(bmim)(PF_6)	1178	596	8.14	32.7	53.6	232.8	0.426

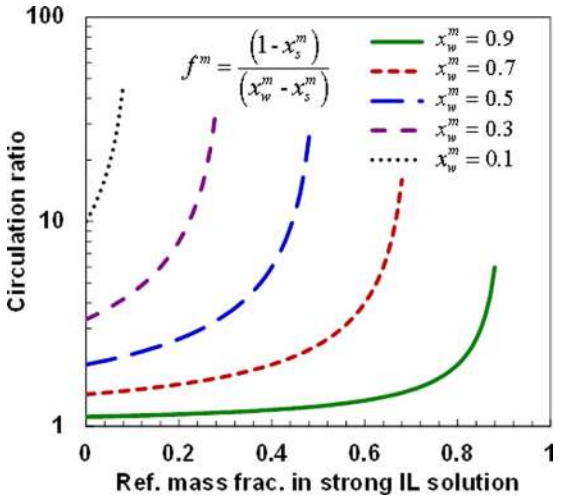

Fig. 10 Circulation ratio with respect to the refrigerant mass fraction in strong-IL solution

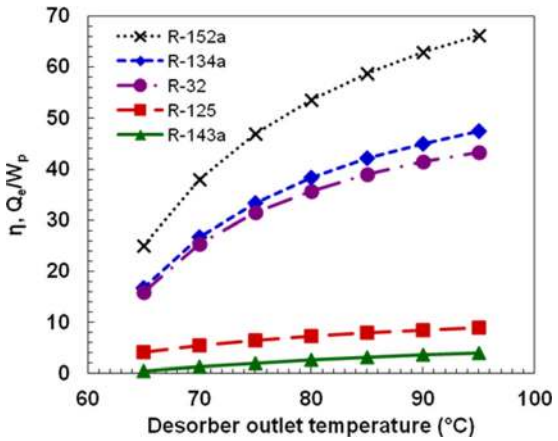

Fig. 11 Desorber outlet temperature effect on efficiency, η, for working fluid (bmim)(PF_6) and HFC refrigerants. $T_c/T_e/T_a = 50/25/35\,^{\circ}C$

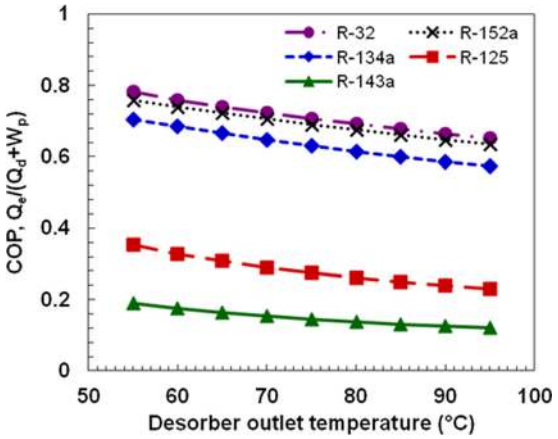

Fig. 12 Effect of absorber temperature on system performance for working fluid (bmim)(PF_6) and HFC refrigerants. $T_c/T_e/T_a = 50/25/26\,^{\circ}C$

requires larger desorber power supply (Q_d) and thus the decrease of COP in Fig. 9. On the other hand, the circulation ratio is decreased by the increase of the desorber outlet temperature that leads to the reduction of the desorber power input. The circulation ratio was determined by Eq. (23):

$$f^m = \frac{m_w}{m_r} = \frac{(1 - x_s^m)}{(x_w^m - x_s^m)} \tag{23}$$

where x_s^m and x_w^m are the mass fractions of refrigerant in the strong- and the weak-IL solutions, respectively. Since as shown in the solubility curves in Figs. 2–6, an increase of the desorber outlet temperature brings about a reduction of refrigerant mass fraction of the strong-IL solution, the circulation ratio is decreased by Eq. (22) (Fig. 10). Pumping power is also reduced due to the decreased solution flow rate (m_w). Finally, both the smaller desorber heat input and the pumping power result in improved CE at an increased desorber outlet temperature. This is, however, in conflict with the effect of the increased desorber outlet enthalpies, which calls for a reduction of CE. The results shown in Fig. 9 suggest that the effect of the desorber outlet temperature increase on the circulation ratio and the solution flow rate is not that profound. Thus, the CE tends to level off from the maximum value, which is likely due to the increase of desorber outlet enthalpies. Note that the CE trends for the five HFC refrigerants examined in Fig. 9 match those of the molar solubility of the refrigerants in (bmim)(PF_6), i.e., R32 > R152a > R134a > R125 > R143a. This result emphasizes the importance of the affinity between absorbent (IL) and refrigerants in order to achieve the highest system performance.

When waste heat can be utilized to supply heat at the desorber, a more practical system COP is defined in Eq. (24):

$$\eta = \frac{Q_e}{W_p} \tag{24}$$

Equation (24) is the more usual figure of merit for absorption refrigeration/heat pump systems where waste heat is used and does not appear in the performance metric. Equation (24) removes the contribution of the heat input at the desorber from the system's thermal efficiency (Eq. (7)). The coefficient of performance η is plotted with respect to desorber outlet temperature in Fig. 11. As previously discussed, at higher desorber outlet temperatures, the pumping work is reduced due to the increase of circulation ratio, which leads to an enhanced system efficiency. When waste (free) heat is provided at the desorber to drive the system, the operating pressure range becomes important as the pumping work is the product of the liquid volumetric flow rate and pressure difference between the absorber and desorber; i.e., $W_p \sim V_l \times \Delta P$. It is surprising that R32 still shows relatively high performance, even though the pressure difference is twice as large as that of R152a and R134a (Table 5). This again suggests that high solubility of a refrigerant in the absorbent should be a primary factor in the selection of working fluids for the cycle.

Once the absorbent/refrigerant are selected, to ensure maximum efficiency of the system, the operating conditions must be optimized for a given pair of working fluids. To that end, the effect of absorber temperature can be observed by comparing Fig. 12 with Fig. 9, where the absorber inlet temperature was lowered from 35 °C to 26 °C. The results show that the COP increases for all HFC refrigerants due to the increased refrigerant solubility at the absorber at lower temperatures. It is more evident from the Raoult's law which gives Eq. (25):

$$x_w \sim \frac{P_e}{P_{sat}(T_5)} \tag{25}$$

At the lower absorber outlet temperature ($T_5 = 26\,^{\circ}C$), the refrigerant mole fraction in the weak-IL solution is increased, resulting in the decrease of the circulation ratio and thus the increase of COP. Another noticeable change is the smaller COP difference between R32, R152a, and R134a. This is

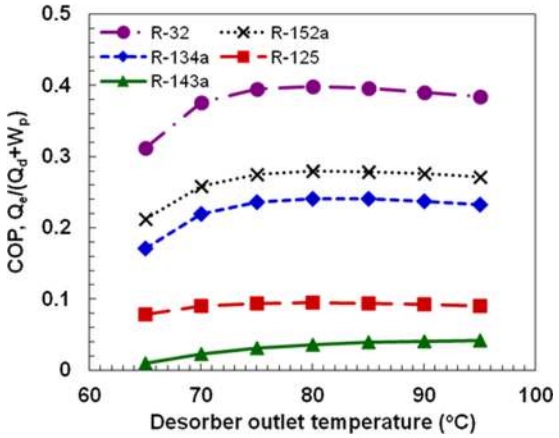

Fig. 13 System performance without the solution heat exchanger for working fluid (bmim)(PF_6) and HFC refrigerants. $T_c/T_e/T_a = 50/25/35$ °C.

because the solubility of all refrigerants saturates in (bmim)(PF_6) at nearly 0.97.

System design is also important for efficient operation of the system. A solution heat exchanger is an essential component, as heat that would be otherwise rejected to the ambient can be recovered to preheat the circulating solution. Therefore, the required heat supply at the desorber will decrease, which would lead to higher system efficiency. To quantify the efficacy of the heat exchanger to the system performance, the CE of a system without a solution heat exchanger was evaluated in Fig. 13. When compared to the results in Fig. 9, in the case of R143a the CE was increased 14-fold and on average the CE was doubled in the presence of the the heat exchanger. Also, it was observed that the CE reaches its maximum at the desorber outlet temperature around 80 °C, which is different from the trend in Fig. 9. When the pressure is fixed, the solubility changes become less sensitive to increasing temperature (Figs. 2–6). This means that the desorber outlet temperature changes have a more significant effect on the solubility, as well as circulation ratio (Eq. (21)) at low desorber outlet temperatures. Therefore, at low desorber outlet temperature, the effect of the circulation ratio decrease is a more dominant mechanism than that of an increased desorber temperature difference, and thus, CE increases. However, at a high desorber outlet temperature, the variation of the circulation ratio is suppressed and the effect of an increased desorber temperature difference becomes dominant, which necessitates an increased desorber power supply and resulting CE decrease.

Figure 14(*a*) shows the experimentally measured CE_{Th} of the absorption refrigeration system using R134a/(bmim)(PF_6) mixture as the working fluid pair. Similar to the predictions in Fig. 13, CE_{Th}s range from 0.1 to 0.4 without solution heat exchanger. Also, the system performance reaches its maximum at the desorber outlet temperatures around 75 °C ~ 80 °C, which is consistent with the theoretical results shown in Fig. 13. Considering that practical imperfections of the system as well as the details of heat/mass exchange processes in the system components have not been fully reflected in the model, the system-level predictions are in fairly good agreement with the experimental data. A more detailed model would be useful for understanding/characterizing the effects of flow maldistributions in microfluidic channel, kinetics of absorption/desorption processes, liquid-vapor separations, and heat exchanger effectiveness. It was observed that with the smaller solution expansion valve opening, the system showed better performance (Fig. 14(*a*)). This is because less desorber power (Q_d) is consumed with the narrowed solution expansion valve flow path, which brings about the reduced solution flow rate (Fig. 14(*b*)). The evaporator cooling capacity increased with increasing desorber outlet temperature (Fig. 14(*c*)), since refrigerant flow rate (m_r) increases with the reduction of the circulation ratio (Eq. (21)). However, as the desorber outlet temperature increases, the circulation ratio reduction by the decrease of x_s^m becomes insignificant (Fig. 10), which results in the saturation of the evaporator cooling capacity enhancement in Fig. 14(*c*). It is interesting that the effect of the expansion valve opening is negligibly small on the evaporator cooling capacity, which needs further study.

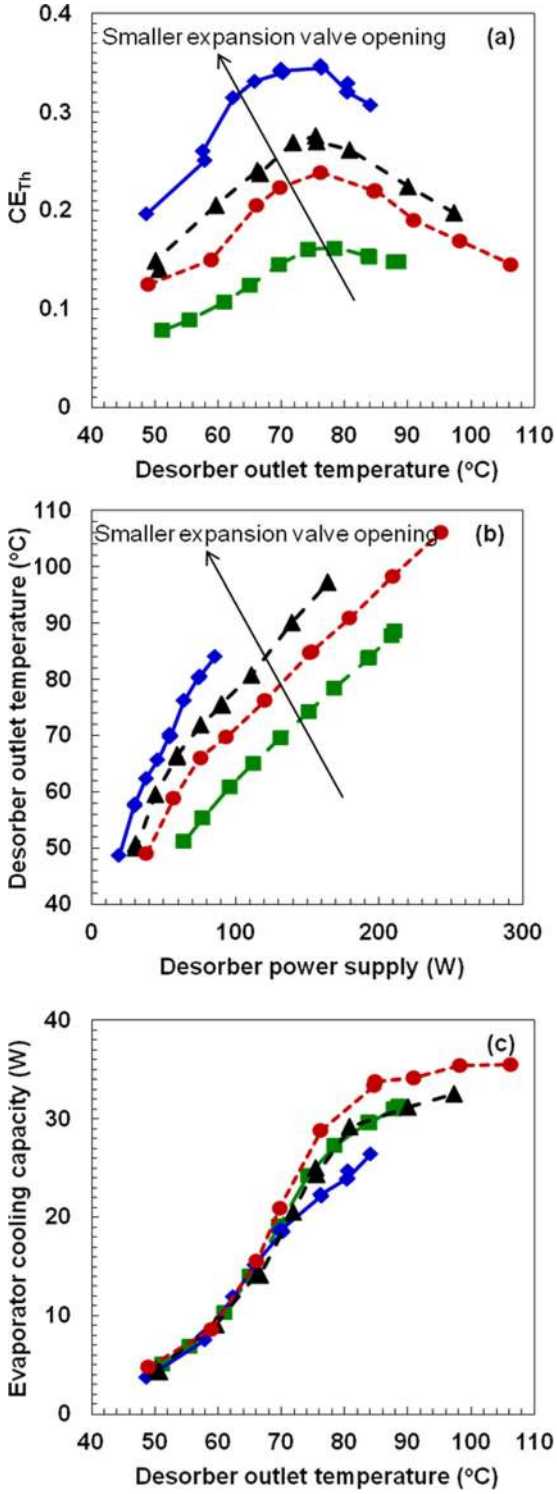

Fig. 14 Experimentally measured (*a*) CE_{Th} and (*c*) evaporator cooling capacity with respect to the desorber outlet temperature and (*b*) the relation between the desorber outlet temperature and desorber power input

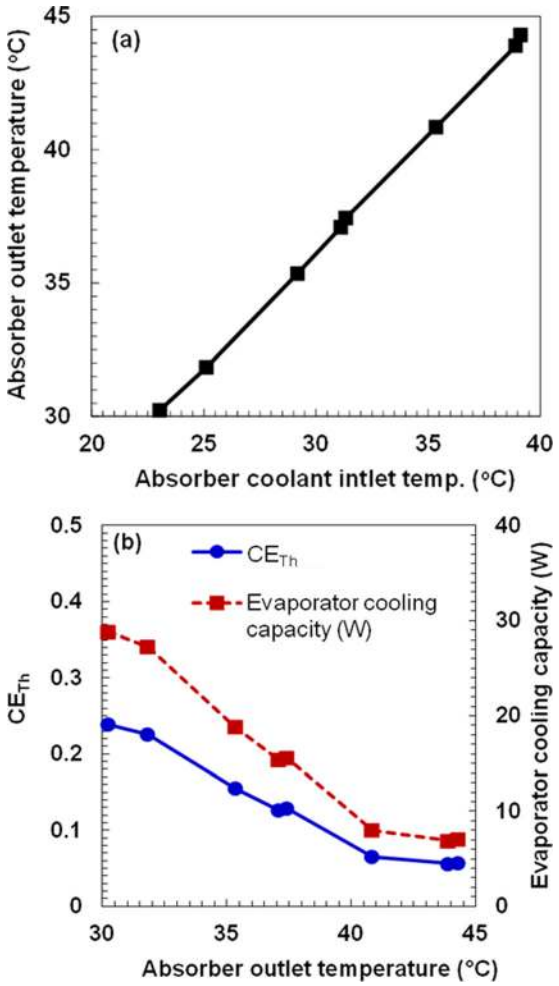

Fig. 15 Experimentally measured (*a*) relation between the absorber outlet temperature and the absorber coolant inlet temperature and (*b*) CE_{Th} with respect to the absorber outlet temperature

Figure 15 shows the effect of the refrigerant inlet temperature variation on the system performance. The absorber outlet temperature changes approximately proportional to the absorber coolant inlet temperature (Fig. 15(*a*)). When the refrigerant inlet temperature varied in the range of 23 °C ~ 39 °C, the absorber outlet temperature varied between 30 °C ~ 44 °C. Both the CE_{Th} and evaporator cooling capacity decrease with increasing absorber outlet temperature, which is attributed to the increase of circulation ratio due to the decrease of the refrigerant mass fraction x_w^m in the weak-IL solution.

5 Conclusion

Ionic liquid (bmim)(PF_6) and five HFC refrigerants were evaluated as working fluid pairs for an absorption refrigeration/heat pump system. The Redlich–Kwong EOS was employed to predict the mixture properties and to define the states of the thermodynamic cycle. The system efficiency showed strong dependency on the affinity between the refrigerant and absorbent. However, when waste heat is available, operating pressure ranges also become an important practical factor that defines the system efficiency. Furthermore, the results show that the operating conditions and system/component designs are essential in order to improve the system performance.

A laboratory scale experimental setup for the absorption heat pump system using R134a/(bmim)(PF_6) mixture as a working fluid was built to evaluate the feasibility of the system. With the desorber outlet temperature ranging from 50 °C to 110 °C, the system was operated with the maximum COP of 0.35 and evaporator cooling capacity of 36 W without a solution heat exchanger. As predicted, adding a solution heat exchanger could boost the COP up to 0.8, and it is expected that the adjustment of the operating conditions can bring further increase of COP. Further studies on the system performance optimization, more efficient desorber and absorber designs, and low vapor pressure, high solubility IL/refrigerant combinations are suggested.

Acknowledgment

The authors acknowledge the support of the Interconnect Focus Center, one of six research centers funded under the Focus Center Research Program, a Semiconductor Research Corporation program.

Nomenclature

CE = cooling-to-total-energy
CE_{Th} = cooling-to-total-thermal energy
COP = coefficient of performance
C_p = ideal-gas heat capacity (J/mol)
f = circulation ratio
H = molar enthalpy (J/mol)
H^R = residual enthalpy (J/mol)
h = specific enthalpy (J/kg)
k, l = adjustable binary interaction parameter
m = mass flow rate (kg/s)
P = pressure (Pa)
Q = heat transfer rate (W)
R = gas constant, 8.314 J/mol·K
T = temperature (K)
V = molar volume (cm^3/mol)
W_p = pumping work (W)
x = liquid phase refrigerant mole fraction
x^m = liquid phase refrigerant mass fraction

Greek Symbols

η = system efficiency utilizing waste heat
τ = adjustable binary interaction parameter (K)
φ = fugacity coefficient

Subscripts

0 = feference state
1,…, 10 = state numbers indicated in Fig. 1
a = absorber
c = condenser
d = desorber
e = evaporator
l = liquid
r = refrigerant
s = strong-ionic liquid solution
sat = saturation
w = weak-ionic liquid solution

References

[1] Brown, R., Nordman, B., Tschudi, B., Shehabi, A., Stanley, J., Koomey, J., Sartor, D., Chan, P., Loper, J., Capana, S., Hedman, B., Duff, R., Haines, E., Sass, D., and Fanara, A., 2008, "Report to Congress on Server and Data Center Energy Efficiency—Public Law 109-431," Lawrence Berkeley National Laboratory, Berkeley, CA.
[2] Pakbaznia, E., and Pedram, M., 2009, "Minimizing Data Center Cooling and Server Power Costs," ISLPED '09: Proceedings of the 14th ACM/IEEE International Symposium on Low Power Electronics and Design, San Fransisco, CA, Aug. 19–21.
[3] Pal, A., Joshi, Y. K., Beitelmal, M. H., and Patel, C. D., 2002, "Design and Performance Evaluation of a Compact Thermosyphon," IEEE Trans. Comp. Pack. Tech., **25**(4), pp. 601–607.

[4] Maydanik, Y. F., Vershinin, S. V., Korukov, M. A., and Ochterbeck, J. M., 2005, "Miniature Loop Heat Pipes—A Promising Means for Electronics Cooling," IEEE Trans. Comp. Pack. Tech., **28**(2), pp. 290–296.
[5] Jiang, L., Mikkelsen, J., Koo, J. M., Huber, D., Yao, S., Zhang, L., Zhou, P., Maveety, J. G., Prasher, R., Santiago, J. G., Kenny, T. W., and Goodson, K. E., 2002, "Closed-Loop Electroosmotic Microchannel Cooling System for VLSI Circuits," IEEE Trans. Comp. Pack. Tech., **25**(3), pp. 347–355.
[6] Wei, Y., and Joshi, Y. K., 2004, "Stacked Microchannel Heat Sinks for Liquid Cooling of Microelectronic Components," ASME J. Electron. Packaging, **126**, pp. 60–66.
[7] Bintoro, J. S., Akbarzadeh, A., and Mochizuki, M., 2005, "A Closed-Loop Electronics Cooling by Implementing Single Phase Impinging Jet and Mini Channels Heat Exchanger," Appl. Therm. Eng., **25**, pp. 2740–2753.
[8] Fan, X., Zeng, G., LaBounty, C., Bowers, J. E., Croke, E., Ahn, C. C., Huxtable, S., Majumdar, A., and Shakouri, A., 2001, "SiGeC/Si Superlattice Microcoolers," App. Phys. Lett., **78**(11), pp. 1580–1582.
[9] Mongia, R., Masahiro, K., DiStefano, E., Barry, J., Chen, W., Izenson, M., Possamai, F., Zimmermann, A., and Mochizuki, M., 2006, "Small Scale Refrigeration System for Electronics Cooling Within a Notebook Computer," Proceedings of the Intersociety Conference on Thermal and Thermomechanical Phenomena in Electronics Systems (I-THERM), San Diego, CA, May 30-June 2, pp. 751–758.
[10] Drost, M. K., and Friedrich, M., 1997, "Miniature Heat Pump for Portable and Distributed Space Conditioning Applications," Proceedings of the 32nd Intersociety Energy Conversion Engineering Conference (IECEC-97), Honolulu, HI, July 27-Aug. 1.
[11] Kim, Y. J., Joshi, Y. K., and Fedorov, A. G., 2008, "An Absorption Based Miniature Heat Pump System for Electronics Cooling," Int. J. Refrig, **31**(1), pp. 23–33.
[12] Suman, S. Joshi, Y., and Fedorov, A., 2004, "Cryogenic/Sub-Ambient Cooling of Electronics: Revisited," Proceedings of the Ninth Intersociety Conference on Thermal and Thermomechanical Phenomena in Electronic Systems (ITHERM '04), Las Vegas, NV, June 1–4.
[13] Srikhirin, P., Aphornratana, S., and Chungpaibulpatana, S., 2001, "A Review of Absorption Refrigeration Technologies," Renew. Sustain. Energ. Rev., **5**(4), pp. 343–372.
[14] Abdelmessih, A. N., Abbas, M., Al-Hashem, A., and Munson, J., 2007, "Ethylene Glycol/Water as Working Fluids for an Experimental Absorption Cycle," Exp. Heat Transfer, **20**(2), pp. 87–102.
[15] Shiflett, M. B., and Yokozeki, A., 2006, "Absorption Cycle Utilizing Ionic Liquid as Working Fluid," U.S. Patent 0197053, pp. 1–47.
[16] Yokozeki, A., 2005, "Theoretical Performances of Various Refrigerant-Absorbent Pairs in a Vapor-Absorption Refrigeration Cycle by the Use of Equations of State," Appl Energ, **80**(4), pp. 383–399.
[17] Shiflett, M., and Yokozeki, A., 2007, "Utilizing Ionic Liquids for Hydrofluorocarbon Separation," U.S. Patent 0131535, pp. 1–42.
[18] Kim, Y. J., Kim, S., Joshi, Y. K., Fedorov, A. G., and Kohl, P. A., "Thermodynamic Analysis of an Absorption Refrigeration System With Ionic-Liquid/Refrigerant Mixture as a Working Fluid," Energy (in press).
[19] Smith, J. M. Van Ness, H. C., and Abbott, M. M., 2005, *Introduction to Chemical Engineering Thermodynamics*, McGraw-Hill, Boston.
[20] Shiflett, M. B., and Yokozeki, A., 2010, "Water Solubility in Ionic Liquids and Application to Absorption Cycles," Ind. Eng. Chem. Res., **49**(19), pp. 9496–9503.
[21] Shiflett, M. B., and Yokozeki, A., 2006, "Solubility and Diffusivity of Hydrofluorocarbons in Room-Temperature Ionic Liquids," AIChE J., **52**(3), pp. 1205–1219.
[22] Yokozeki, A., and Shiflett, M. B., 2006, "Global Phase Behaviors of Trifluoromethane in Ionic Liquid (bmim)(PF_6)," AIChE J., **52**(11), pp. 3952–3957.